Infrared Action Spectroscopy and Inelastic Recoil Dynamics of the CH_4−OD Reactant Complex

Maria Tsiouris, Ilana B. Pollack, and Marsha I. Lester*

Department of Chemistry, University of Pennsylvania, Philadelphia, Pennsylvania 19104-6323

Received: April 5, 2002; In Final Form: June 11, 2002

A rotationally resolved infrared spectrum of the pure OD overtone band of the CH_4−OD reactant complex has been observed at 5165.68(1) cm^{-1}, shifted −9.03(1) cm^{-1} from the infrared overtone transition of OD. The spectrum exhibits homogeneous line broadening, which is estimated to have a zero power line width of 0.10(1) cm^{-1}, corresponding to a lifetime for CH_4−OD ($2\nu_{OD}$) of 53(5) ps. The OD ($\upsilon = 1$) product distribution from vibrational predissociation of the complex favors high rotor levels, indicating that the correlated CH_4 fragment is produced with one quantum of bending excitation. The CH_4−OD results are compared with previous studies in this laboratory of the CH_4−OH complex, and reveal significant changes in lifetime and vibrational predissociation mechanism upon deuteration.

I. Introduction

The work presented here on the CH_4−OD reactant complex is an extension of previous investigations in this laboratory of the CH_4−OH complex. These studies were based on infrared and Raman spectroscopic methods in the OH stretch and the CH_4 symmetric and antisymmetric stretching regions as well as electronic excitation in the OH $A\,^2\Sigma^+ - X\,^2\Pi$ (1,0) region.[1−3] The earlier studies determined the structure, stability, and vibrational decay dynamics of CH_4−OH complexes that have been trapped in the entrance channel to the fundamental $CH_4 + OH \rightarrow CH_3 + H_2O$ hydrogen abstraction reaction, as illustrated in Figure 1. The goal of the present study is to examine the changes in the spectroscopic properties and decay dynamics of the complex upon deuteration of the hydroxyl moiety.

Infrared spectra of the CH_4−OH complex have previously been obtained in the OH fundamental and overtone regions.[2] Structural parameters derived from the rotationally resolved spectra indicated that the centers of mass of the CH_4 and OH partners are separated by $R = 3.66(1)$ Å.[4] In addition, the projection quantum number showed that the OH bond axis lies along the intermolecular axis in the ground state of CH_4−OH. Previous electronic spectroscopy measurements also indicated a ground-state binding energy of $D_0 \sim 0.6$ kcal/mol.[1] These experimental observations were consistent with complementary ab initio calculations performed at the MP2-aug-cc-pVTZ level that predict a $C_{3\nu}$ minimum energy configuration for CH_4−OH with the hydrogen of OH pointing toward one of four equivalent faces of the CH_4 tetrahedron at an equilibrium separation distance of $R_e = 3.47$ Å and a well depth of $D_e \sim 1$ kcal/mol,[2] as depicted in Figure 1. This is also the structure adopted by many CH_4−HX closed shell analogues, where X = F, Cl, Br, and CN.[5−10] Very recently, Hashimoto and Iwata reported a different minimum energy structure for the CH_4−OH reactant complex, optimized at the UMP2 level, in which the oxygen of OH points toward methane in a more conventional H_3C−H−O−H hydrogen bonded structure.[11] However, these ab initio calculations predict a shallower entrance channel well ($D_e \sim$ 0.5 kcal/mol) and longer separation distance ($R_e = 3.84$ Å) between the centers of mass of the CH_4 and OH reactants than observed experimentally.

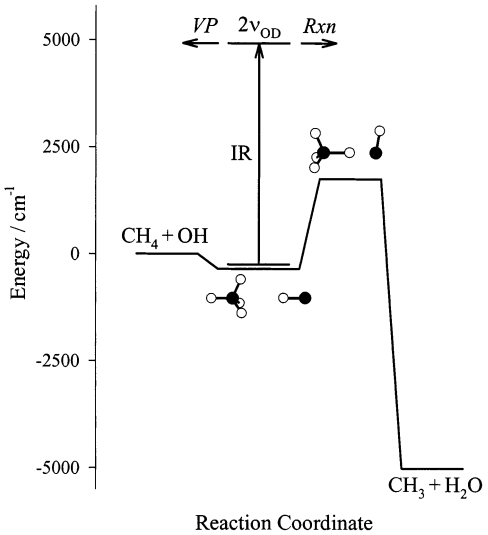

Figure 1. Schematic reaction pathway for $CH_4 + OH \rightarrow CH_3 + H_2O$. The properties of the transition state are obtained from ab initio theory,[36,37] while those of the reactant complex are determined from this and previous studies.[2] In this work, the CH_4−OD isotopomer is characterized spectroscopically using infrared radiation at 1.9 μm, which promotes the complex from its zero-point level to a vibrational level with two quanta of OD stretch ($2\nu_{OD}$). The infrared excitation also provides enough energy to surmount the barrier to reaction (Rxn) or break the weak intermolecular bond via vibrational predissociation (VP).

The infrared spectra in the OH stretching regions also exhibited homogeneous line broadening arising from the rapid decay of vibrationally activated CH_4−OH complexes due to vibrational predissociation and/or reaction. Homogeneous line widths of 0.14(2) and 0.21(2) cm^{-1} have been observed for the pure OH stretching bands in the fundamental and overtone regions, corresponding to 38(5) and 25(3) ps lifetimes for vibrationally activated complexes with one and two quanta of OH stretching excitation, respectively. These lifetimes are

* Author to whom correspondence should be addressed. Fax: (215) 573-2112. E-mail: milester@sas.upenn.edu.

10.1021/jp0209143 CCC: $22.00
Published on Web 07/25/2002

surprisingly short and suggest that both inelastic and reactive channels contribute to the rapid decay of CH_4−OH (ν_{OH}) and ($2\nu_{OH}$) as found in a recent collision study of OH ($\upsilon = 1, 2$) + CH_4.[12] In this study, Yamasaki et al. reported that the rate coefficients for reaction and vibrational deactivation are of comparable magnitude for OH ($\upsilon = 1, 2$) + CH_4,[12] with total rates of removal at 298 K that are 90- or 300-fold greater than found for OH ($\upsilon = 0$) + CH_4 ($k^{OH} = 6.3 \times 10^{-15}$ cm^3 molecule s^{-1}).[12−15] The nascent distribution of the OH products from vibrational predissociation of CH_4−OH ($2\nu_{OH}$) also showed that the dominant inelastic decay channel involves the transfer of one quantum of OH stretch to the pentad of CH_4 vibrational states with energies near 3000 cm^{-1}.

Additional studies have focused on the infrared spectroscopy and subsequent decay dynamics of CH_4−OH reactant complexes in the CH_4 antisymmetric stretching region (ν_3) at 3.3 μm.[3] Infrared excitation of the CH_4 ν_3 mode resulted in an intense, yet enormously broad spectrum extending over 40 cm^{-1}. The appearance of the spectrum has been explained in terms of a model in which the CH_4 unit is freely rotating within the CH_4−OH complex, as found for other CH_4 complexes.[16] In the ν_3 region, the CH_4−OH complex can undergo a multitude of possible transitions, each associated with a rovibrational transition of free methane, which give rise to the enormous span of the CH_4−OH spectrum. The spectrum also exhibited extensive homogeneous broadening ($\geq$1 cm^{-1}) arising from the rapid decay of vibrationally activated CH_4−OH complexes due to vibrational predissociation and/or reaction. This broadening is consistent with quantum reactive scattering calculations that predict a large enhancement in the CH_4 + OH reaction rate in full collisions upon vibrational activation of the C−H stretching mode.[17] The OH fragments from CH_4−OH (ν_3) were produced with minimal rotational excitation, indicating that vibrational predissociation proceeds via near-resonant vibrational energy transfer within the CH_4 unit from the initially prepared asymmetric stretch (ν_3) to an overtone bend ($2\nu_4$) state.

The present study explores the infrared spectrum and vibrational decay dynamics of the partially deuterated CH_4−OD reactant complex. Deuteration of OH is expected to change the dominant inelastic scattering channel resulting from vibrational excitation of the CH_4−OH complex in the OH/D stretching region. The significantly lower vibrational frequency of OD will cause the near-resonant vibrational energy pathway from OH to the pentad of CH_4 states near 3000 cm^{-1} to become energetically closed for CH_4−OD ($2\nu_{OD}$). This should dramatically slow the rate of vibrational predissociation in the deuterated complex based on energy gap arguments. It is also likely to impact on the branching between inelastic and reactive scattering channels, assuming that the rate of reaction is only slightly changed upon deuteration of OD, as found in full collision studies of the OH/D + CH_4 reaction. Indeed, previous kinetic studies have shown that the rate of reaction for ground-state OD radicals with CH_4 is relatively slow at 298 K ($k^{OD} = 6.8 \times 10^{-15}$ cm^3 molecule^{-1} s^{-1}) and is nearly unchanged from that for OH radicals.[13]

II. Experimental Method

An IR pump−UV probe technique has been implemented to obtain the infrared overtone spectrum of CH_4−OD as well as the OD product state distribution resulting from vibrational predissociation of the complex. The IR pump laser prepares CH_4−OD with two quanta of OD vibrational excitation ($2\nu_{OD}$). The UV probe laser then detects the OD ($\upsilon = 1$) fragments from vibrational predissociation on the $A\ ^2\Sigma^+ - X\ ^2\Pi$ (0,1) transition, resulting in a laser-induced fluorescence (LIF) signal.

The CH_4−OD reactant complexes were produced using a procedure similar to that described previously for CH_4−OH complexes.[1−3] The OD radicals were generated by the 193 nm photolysis of commercially available DNO_3 (65 wt %, Aldrich) entrained in a 10% CH_4, balance He carrier gas (150 psi). Photolysis was achieved using an ArF excimer laser (Lambda Physik EMG 101 MSC) at the early stages of a pulsed supersonic expansion. Note that in previous CH_4−OH experiments, the OH radicals were generated using 90 wt % HNO_3 (Aldrich). The lower concentration DNO_3 has a significantly reduced vapor pressure (30 times smaller at 25 °C)[18] and results in lower number densities of photolytically generated OD radicals and CH_4−OD complexes.

A single-mode KTP-based optical parametric oscillator (OPO) (Continuum Mirage 3000) pumped by the output of an injection seeded Nd:YAG laser (Continuum 8000, 10 Hz repetition rate, 7 ns pulse width) provided the tunable infrared radiation. The OPO laser system produces up to ~15 mJ/pulse of 1.9 μm radiation (0.02 cm^{-1} bandwidth), which is used to excite CH_4−OD in the OD overtone region. Additional information regarding single-mode operation of this OPO has been published previously.[2,3,19,20] An absolute calibration for the IR pump laser was obtained by recording an NH_3 photoacoustic spectrum simultaneously with each CH_4−OD infrared scan and comparing it with the well-documented transitions associated with the $\nu_3 + \nu_4$ band of NH_3.[21,22]

The UV probe beam at ~335 nm was generated by the frequency doubled output (KDP) of a Nd:YAG pumped dye laser (Continuum 7020 and ND6000, 20 Hz repetition rate, 7 ns pulse width) operating with a LDS 698/DCM dye mix. Typically, around 1−2 mJ/pulse of UV radiation was utilized. The UV laser was calibrated using the well-known frequencies of the OD monomer in the $A-X$ (0,1) region.[23]

The IR pump and UV probe beams were counterpropagated into the vacuum apparatus, where they were separately focused and then spatially overlapped 1.5 cm downstream of the nozzle exit. The resultant LIF signal was detected with a photomultiplier tube (EMI 9813Q) positioned perpendicular to both the laser and supersonic expansion axes. A number of filters were used to block scattered light arising from the ArF and UV lasers, while still passing OD $A-X$ (0,0) fluorescence at 307 nm. The LIF signal was preamplified, integrated, and transferred to a laboratory computer for analysis. The IR and UV lasers were synchronized such that the IR laser pulse (10 Hz) was present for every other UV pulse (20 Hz), with the UV laser typically arriving in the interaction region 50 ns after the IR pulse. An active background subtraction procedure was implemented, in which any background LIF signal arising from the UV laser alone was subtracted from the combined IR + UV signal on alternating laser pulses. Typically, the LIF signals arising from 150 laser shots (75 IR + UV, 75 UV only) were collected and averaged for each data point.

III. Results

A. Infrared Spectroscopy. Infrared action spectroscopy was utilized to record the infrared spectrum of CH_4−OD in the OD overtone region ($\Delta\upsilon = 2$). This technique relies on vibrational predissociation of CH_4−OD ($2\nu_{OD}$) and the subsequent formation of OD $X\ ^2\Pi$ ($\upsilon = 1$) fragments that are detected by LIF. The IR action spectrum displayed in the bottom panel of Figure 2 was obtained with the UV probe laser fixed on the OD $A-X$ (0,1) $Q_1(17/2)$ transition.[23] The optimum UV probe transition was chosen empirically based on the magnitude of the IR induced signal. The IR spectrum of CH_4−OD is located at

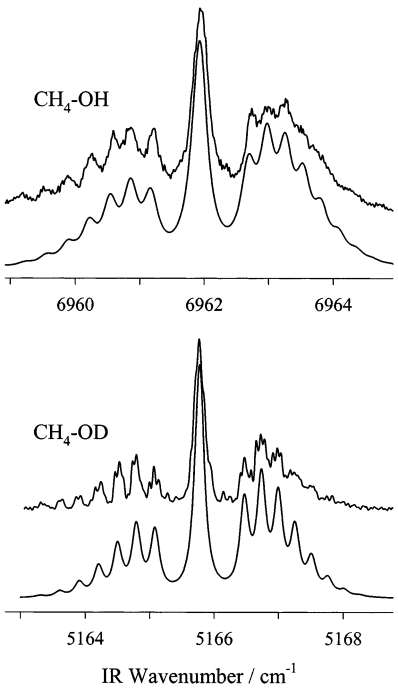

Figure 2. Rotationally resolved infrared spectrum of the pure OD overtone band of CH_4-OD (bottom) and the analogous spectrum of CH_4-OH obtained in the OH overtone region (top).[2] Below each experimental spectrum is a simulation generated by the fitting procedure described in the text. The CH_4-OH spectrum exhibits more extensive homogeneous linebroadening (0.24(2) cm^{-1}) than seen in the CH_4-OD spectrum (0.13(2) cm^{-1}) at comparable IR pump energies of ~5 mJ/pulse. The IR pump energy was systematically decreased to obtain the lifetime broadening contribution to the line width.

5165.68(1) cm^{-1} (band origin), shifted 9.03(1) cm^{-1} to lower energy of the OD Q(3/2) transition.[24] This spectrum is attributed to the pure OD overtone band of CH_4-OD based on its proximity to the OD overtone transition and its similarity to the pure OH overtone band of CH_4-OH.[2] The previously reported infrared spectrum of CH_4-OH in the OH overtone region is also shown in Figure 2 (top) for comparison.

The spectral shift of the pure OD overtone transition of CH_4-OD, −9.03(1) cm^{-1}, is nearly equivalent to that of the pure OH overtone transition of CH_4-OH, which was observed 9.37(1) cm^{-1} to lower energy of the OH Q(3/2) transition. This indicates similar decreases in the OH/D vibrational frequencies upon complexation with CH_4 (0.13% for OH and 0.17% for OD). The spectral shifts are also a measure of the decrease in binding energies for CH_4-OH and CH_4-OD upon OH/D vibrational overtone excitation.

The rotational structure of the pure overtone band of CH_4-OD is characterized by an unresolved Q-branch and partially resolved P- and R-branches, which has the same appearance as the pure overtone spectrum of CH_4-OH. The ~5B gaps on either side of the central Q-branch as well as the ~2B regular spacing between adjacent P-branch and R-branch lines are indicative of a parallel ($P' = 3/2$)−($P'' = 3/2$) transition. Here, P refers to the projection of the total angular momentum J along the intermolecular axis. The nonzero value of P arises from the unquenched angular momentum of OD, which has a projection $\omega = 3/2$ on the OD bond axis and will give rise to a projection $P = 3/2$ when the OD bond axis is oriented on average along the intermolecular axis. As discussed previously in detail for CH_4-OH, the magnitude of P is determined solely from the internal angular momentum of the OH/D partner with no contribution from CH_4, which undergoes nearly free internal rotation within the complex.[2,3]

TABLE 1: Spectroscopic Parameters (cm^{-1}) Derived from the Pure OH/D Overtone Bands of CH_4-OH and CH_4-OD (The distances R (Å) between the centers of mass of OH/D and CH_4 are also listed. Values in parentheses are 1σ uncertainties.)

parameter	CH_4-OH[a]	CH_4-OD
origin, ν_0	6961.97(1)	5165.68(1)
shift from OH/D Q(3/2)[b]	−9.37(1)	−9.03(1)
B''	0.151(1)	0.144(1)
B'	0.147(1)	0.142(1)
R	3.66(1)[c]	3.69(1)
homogeneous line width, fwhm[d]	0.21(2)	0.10(1)
D_0	210(20)	≤ 293

[a] Spectroscopic data for CH_4-OH is reproduced from ref 2. [b] Value averaged over two λ doublet components (refs 23, 26). [c] See ref 4. [d] Based on extrapolation of the observed homogeneous line width to the limit of zero power.

A least-squares fitting procedure has been performed in which the ground and excited-state rotational constants, B'' and B', respectively, and band origin, ν_0, were varied in order to minimize the sums of the squares of the residuals between the observed and calculated line positions. This fitting procedure yields a rotational constant of $B'' = 0.144(1)$ cm^{-1} for the ground state of CH_4-OD, corresponding to a separation between the centers of mass of CH_4 and OD of $R'' = 3.69(1)$ Å. A rotational constant of $B' = 0.142(1)$ cm^{-1}, which corresponds to $R' = 3.72(1)$ Å, was determined for CH_4-OD ($2\nu_{OD}$) indicating no significant change in either the rotational constant or the separation between the centers of mass of the CH_4 and OD partners upon OD overtone excitation. In addition, spectral simulations of the band contour based on a parallel ($P' = 3/2$)−($P'' = 3/2$) transition for a pseudo-diatomic molecule were carried out to determine the Lorentzian line width of the band.[25] The best fit is shown in Figure 2 directly below the experimental spectrum. The spectroscopic parameters determined for CH_4-OD along with those derived from an equivalent analysis of the pure overtone band of CH_4-OH are presented in Table 1.

The separation between the centers of mass of CH_4 and OH/D in the ground state complex is found to be nearly unchanged upon deuteration, changing from $R = 3.66(1)$ to 3.69(1) Å. On the basis of the minimum energy structure predicted from ab initio calculations[2] with the H/D atom of the hydroxyl radical pointing toward CH_4, we anticipated observing a 0.054 Å decrease in distance between the centers of mass upon deuteration. This follows from the 0.054 Å decrease in the distance between the H/D atom and the center of mass of hydroxyl radical for OD as compared to OH.[23,26] Since this decrease is not observed, it suggests that OH/D is undergoing wide amplitude motion, consistent with its small binding energy to CH_4, and is not locked into position along the intermolecular axis. Alternatively, if the O atom of the hydroxyl radical points toward CH_4, as suggested by the ab initio calculations of Hashimoto and Iwata,[11] then the separation between the centers of mass of CH_4 and OH/D should increase slightly upon deuteration as observed. However, these calculations also predict a larger separation distance than observed experimentally for either isotopomer. In both of the calculated structures, the OH radical will have a well-defined projection of $P = 3/2$ along the intermolecular axis, as observed experimentally.

B. Spectral Line Widths. Both the CH_4-OH and CH_4-OD pure overtone spectra (Figure 2) exhibit line widths that are much greater than the 0.02 cm^{-1} bandwidth of the infrared laser source. As can be seen in Figure 2, CH_4-OH shows even

more extensive line broadening than CH_4−OD, with homogeneous line widths of 0.24(2) and 0.13(2) cm^{-1}, respectively, at an IR pump energy of ∼5 mJ/pulse. To determine if this spectral broadening arises from saturation broadening due to the high infrared pump power or lifetime broadening, the pure overtone spectrum of the CH_4−OD complex was recorded several times while systematically decreasing the IR pump energy. As the IR pulse energy was lowered, the line width observed for CH_4−OD decreased from 0.15(2) cm^{-1} at ∼15 mJ to 0.10(1) cm^{-1} at ∼2.5 mJ. At energies lower than 2.5 mJ, the line width could not be determined due to the significantly reduced signal-to-noise ratio of the spectral data. Therefore, to estimate the lifetime broadening contribution to the line width, the data was linearly extrapolated to zero power. This extrapolation yields an upper limit of 0.10(1) cm^{-1} for the lifetime broadening component of the spectral line width, which corresponds to a lower limit for the lifetime of approximately 53(5) ps for CH_4−OD ($2\nu_{OD}$). A similar extrapolation carried out previously for CH_4−OH ($2\nu_{OH}$) yielded an upper limit of 0.21(2) cm^{-1} for the lifetime broadening component of the spectral line width, corresponding to a lower limit for the lifetime of 25(3) ps.[2] Thus, the work presented here indicates an approximate 2-fold increase in the lifetime of vibrationally activated CH_4−OH upon deuteration. This lifetime is inversely related to the sum of the unimolecular decay rates for vibrational predissociation and chemical reaction.

The lifetimes determined for both CH_4−OH and CH_4−OD upon OH/D overtone excitation are surprisingly short in comparison to other diatom−polyatom complexes such as C_2H_2−HCl[27] and CO_2−HF,[28] which have vibrationally excited lifetimes in excess of 100 ps. Furthermore, the lifetimes for CH_4−OH/D are significantly shorter than seen for other OH complexes including OH/D−N_2 and OH/D−CO,[20,29] where the lifetimes are on a nanosecond time scale and increase by a factor of 5 or more upon deuteration. These two issues, rapid decay rates for CH_4−OH ($2\nu_{OH}$) and CH_4−OD ($2\nu_{OD}$) as well as the 2-fold change in decay rate upon deuteration, will be discussed after we consider the quantum state distribution of the products.

C. OD Product State Distribution. The inelastic recoil dynamics of the OD + CH_4 fragments were also examined by measuring the OD product state distribution following vibrational predissociation of CH_4−OD ($2\nu_{OD}$). For these measurements, the IR laser was fixed on the Q-branch of the pure overtone band of CH_4−OD at 5965.7 cm^{-1} and the UV probe laser was scanned over various OD $A-X$ (0,1) transitions (Q_1, Q_2, R_1, and R_2 branches).[23] These particular transitions were chosen in order to examine the relative population of the OD ($v = 1$) fragments as a function of rotational (j_{OD}), spin−orbit (ω), and lambda (λ)-doublet state. The intensities observed for each of the OD probe transitions were scaled relative to the OD $Q_1(17/2)$ line, which was scanned immediately before and after every other line. The measurements of OD transition intensities were performed in the fully saturated LIF regime and appropriately converted into relative populations of OD ($v = 1$) rotational levels.[30−32] Populations derived from Q- or R-branch lines originating from the same j_{OD} were nearly identical (within the experimental uncertainty) indicating no λ-doublet propensity. In addition, no spin−orbit propensity was observed since the populations derived from the satellite branches (Q_2, R_2) were the same as those extracted from the main branches (Q_1, R_1) for each j_{OD} state.

The bottom panel of Figure 3 shows the relative population of OD ($v = 1$) fragments as a function of the OD ($v = 1$) internal energy (rotational and spin−orbit) for both the $\omega = 3/2$ (filled circles) and $\omega = 1/2$ (open circles) spin−orbit manifolds after summing over λ-doublet components. The ticks identify the j_{OD} states probed in each spin−orbit manifold. The OD ($v = 1$) population is observed to grow with increasing internal excitation of OD, reaching a maximum at $j_{OD} = 17/2$, $\omega = 3/2$, and $j_{OD} = 15/2$, $\omega = 1/2$. For these most populated product states, the OD ($v = 1$) fragments are released with approximately 700 or 765 cm^{-1} of internal energy. At higher OD ($v = 1$) fragment internal energies, the distribution falls off sharply and no population is observed for $j_{OD} > 17/2$, $\omega = 1/2$. The lowest rotational level of the lower spin−orbit manifold, $j_{OD} = 3/2$, $\omega = 3/2$, could not be probed due to its large background population in the supersonic expansion. Additionally, the lowest rotational levels of the upper spin−orbit component, $j_{OD} < 9/2$, $\omega = 1/2$, could not be investigated, owing to interference from overlapping OD lines.

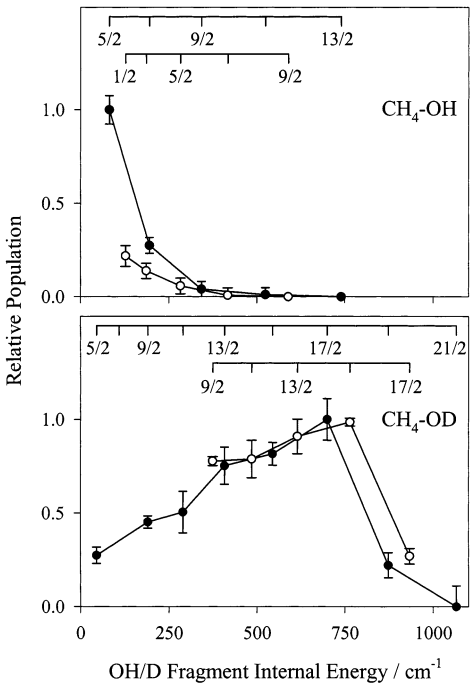

Figure 3. The OD ($v = 1$) product state distribution resulting from vibrational predissociation of CH_4−OD ($2\nu_{OD}$) (bottom). The OD fragment distribution peaks at $j_{OD} = 17/2$ in the lower ($\omega = 3/2$) spin−orbit manifold (filled circles) and $j_{OD} = 15/2$ in the upper ($\omega = 1/2$) spin−orbit manifold (open circles) with no population observed in OD internal energy states with $j_{OD} > 17/2$, $\omega = 1/2$. By contrast, vibrational predissociation of CH_4−OH ($2\nu_{OH}$) results in a distinctly different OH fragment distribution (top). The OH ($v = 1$) population peaks in the lowest observed $j_{OD} = 5/2$, $\omega = 3/2$ and $j_{OD} = 1/2$, $\omega = 1/2$ levels and decreases steadily with increasing OH fragment internal (rotational and spin−orbit) energy.

A remarkably different product state distribution was observed previously for CH_4−OH ($2\nu_{OH}$) as shown in the top panel of Figure 3. In this case, the OH ($v = 1$) fragments are produced with minimal rotational excitation. The OH ($v = 1$) product state distribution peaks at the lowest observed levels $j_{OD} = 5/2$, $\omega = 3/2$, and $j_{OD} = 1/2$, $\omega = 1/2$ and steadily decreases with increasing OH fragment internal energy. As discussed in ref 2, the minimal internal excitation of the OH ($v = 1$) fragments reveals that most of the available energy is used to populate excited CH_4 vibrational states, namely the pentad of vibrational states near 3000 cm^{-1}. The dramatic change in the OH/D product state distribution indicates a significant change in the vibrational predissociation dynamics upon deuteration.

The OD ($v = 1$) fragment distribution also provides limited information about the vibrational state distribution of the

correlated CH_4 fragment as well as the ground-state binding energy of the complex (D_0). An energy balance equation can be used to show the relationship between the IR excitation and binding energies of the CH_4-OD complex (LHS), and the energy released to OD and CH_4 fragments as vibrational, internal (rotation or spin−orbit), and translational energy (RHS):

$$CH_4-OD\ (2\nu_{OD}) - D_0 = OD\ (\upsilon = 1, j_{OD}, \omega) + CH_4\ (\nu_i, j_{CH_4}) + E_{trans}$$

In applying this relationship, we will make the assumptions that energy accommodation in CH_4 rotation is small ($j_{CH_4} \sim 0$) and E_{trans} is minimized.[33,34] Thus, for each OD ($\upsilon = 1$) product state observed, we can deduce some constraints on D_0 and the vibrational states of the CH_4 partner that can be populated.

When OD ($\upsilon = 1$) fragments are produced in their highest observed internal energy state, $j_{OD} = 17/2$, $\omega = 1/2$, approximately 1600 cm^{-1} of energy is available for breaking the CH_4-OD intermolecular bond (D_0) and vibrational excitation of the CH_4 partner. This is not sufficient energy to produce CH_4 fragments in the pentad of vibrational states near 3000 cm^{-1}, as was observed following vibrational predissociation of CH_4-OH ($2\nu_{OH}$).[2] Nor is it sufficient energy to produce CH_4 with ν_2 bend (1526 cm^{-1}), since this would imply an unrealistically small binding energy for CH_4-OD ($D_0 = 74$ cm^{-1}). However, there is enough energy to produce CH_4 fragments with ν_4 bending excitation (1306 cm^{-1}) and still obtain a realistic estimate for the CH_4-OD binding energy of $D_0 = 294$ cm^{-1}. This limit is consistent with the binding energy for CH_4-OH, previously determined to be 210 ± 20 cm^{-1} from electronic spectroscopy experiments,[1] which is expected to increase upon deuteration of the hydroxyl partner. It is also in accord with the decrease in zero-point energy of $\sim$60 cm^{-1} estimated for the intermolecular modes of CH_4-OH (see Table 3 of ref 2), in particular, the OH bend, upon deuteration.

At the peak of the OD ($\upsilon = 1$) product state distribution, $j_{OD} = 17/2$, $\omega = 3/2$, and for all lower internal energy states, there is enough energy available to produce CH_4 fragments with either ν_2 or ν_4 bending excitation. The next most populated fragment state, $j_{OD} = 15/2$, $\omega = 1/2$, would not leave sufficient energy to populate the CH_4 ν_2 bending state unless the CH_4-OD binding energy was reduced to a somewhat lower but still reasonable value of $D_0 \leq 243$ cm^{-1}. (Nevertheless, we report only an upper limit for the binding energy of CH_4-OD of $D_0 \leq 294$ cm^{-1}.) The sudden drop in the OD ($\upsilon = 1$) product distribution beyond these most populated states suggests the closing of a near-resonant product channel, namely, vibrational energy transfer from OD to the CH_4 ν_2 bending state. The overall cutoff of the OD ($\upsilon = 1$) product rotational distribution suggests that the ν_2 and ν_4 bending states are the most favorable vibrational states of the CH_4 products.

IV. Discussion

The quantum state distributions observed for the OH and OD fragments reveal a dramatic change in the vibrational predissociation dynamics upon deuteration. An energy level diagram depicting the vibrational predissociation mechanisms for CH_4-OH/D is shown in Figure 4. Vibrational activation of the OH overtone in CH_4-OH yields CH_4 ($2\nu_2$) and OH ($\upsilon = 1$) products with very little excess energy available for rotational and/or translational excitation of the fragments. The latter quantity, often termed the energy gap,[33,34] is only 120 cm^{-1} for CH_4-OH ($2\nu_{OH}$), since vibrational predissociation takes place through a near-resonant vibrational energy transfer process from OH to

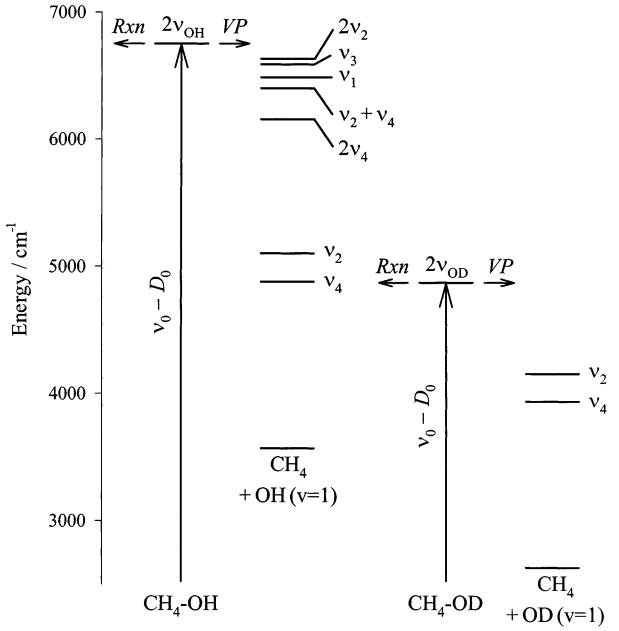

Figure 4. Energy level diagram illustrating the product vibrational levels that are energetically accessible following vibrational predissociation of CH_4-OH ($2\nu_{OH}$) and CH_4-OD ($2\nu_{OD}$). Vibrational predissociation of CH_4-OH ($2\nu_{OH}$) proceeds via a near-resonant vibrational energy transfer process to produce OH ($\upsilon = 1$) + CH_4 ($2\nu_2$), and leaves very little excess energy for rotational and/or translational excitation of the fragments. This channel is closed for CH_4-OD ($2\nu_{OD}$) due to the significantly lower vibrational frequency of OD and increased binding energy (D_0) of CH_4-OD. In this case, vibrational energy is transferred from OD to the ν_2 or ν_4 bending vibrations of CH_4, with much more energy available for rotational and/or translational excitation of the fragments.

CH_4. The significantly lower OD vibrational frequency and slightly increased binding energy in CH_4-OD closes this near-resonant process. Instead, vibrational predissociation of CH_4-OD ($2\nu_{OD}$) produces OD ($\upsilon = 1$) + CH_4 (ν_2 or ν_4) fragments, leaving much more energy available for rotational and/or translational excitation of the fragments, specifically an energy gap of at least 715 cm^{-1}. The OD product state distribution shows that much of this excess energy can be accommodated as OD rotational excitation. The larger energy gap for CH_4-OD ($2\nu_{OD}$) immediately suggests that the rate of vibrational predissociation, which is only one component of the total decay rate, will be slower for the deuterated complex.

A 5-fold decrease in the decay rate was observed previously upon deuteration of $OH-N_2$,[20] a system composed of unreactive partners that can decay only by vibrational predissociation. Predissociation of $OD-N_2$ ($2\nu_{OD}$) leaves more than 2000 cm^{-1} for rotational and/or translational excitation of the OD ($\upsilon = 1$) + N_2 ($\upsilon = 0$) fragments,[20] whereas for $OH-N_2$ ($2\nu_{OD}$) only $\sim$800 cm^{-1} of excess energy remains after vibrational energy transfer from OH to N_2.[35] In this system, the decrease in decay rate upon deuteration can be attributed solely to the change in energy gap.

If vibrational predissociation were the only decay channel for CH_4-OH ($2\nu_{OH}$), then the 2-fold increase in lifetime observed upon deuteration would necessarily result from the increase in the energy gap associated with the inelastic decay channel. Since reaction may also contribute to the decay of CH_4-OH ($2\nu_{OH}$) and CH_4-OD ($2\nu_{OD}$), the observed increase in lifetime upon deuteration must correspond to the change in the total decay rate k_T or ($k_{VP} + k_{RXN}$) as follows

$$\frac{\tau^{OD}}{\tau^{OH}} = \frac{k_T^{OH}}{k_T^{OD}} = \frac{(k_{VP}^{OH} + k_{RXN}^{OH})}{(k_{VP}^{OD} + k_{RXN}^{OD})} \approx 2$$

Because the measured lifetime reflects the total decay rate, we can only speculate as to how the individual rate coefficients k_{VP}^{OH} and k_{RXN}^{OH} change upon deuteration of OH. We start by *assuming* that the rate coefficient for reaction within the CH_4−OH ($2\nu_{OH}$) complex is comparable to that for vibrational predissociation, $k_{VP}^{OH} \approx k_{RXN}^{OH}$, as found for reaction and vibrational deactivation in full collision studies of OH ($v = 2$) + CH_4.[12] The rapid decay of CH_4−OH ($2\nu_{OH}$) may be a result of such a substantial contribution (∼50%) from reaction. If we also *assume* that the rate coefficient for reaction within the complex remains essentially unchanged upon deuteration, $k_{RXN}^{OD} \approx k_{RXN}^{OH}$, as shown in kinetic studies of ground-state OH/D + CH_4 at room temperature[13] but not yet measured for vibrationally excited OD, then the above equation will reduce to $\{(2k_{RXN}^{OH})\}/\{(k_{VP}^{OD} + k_{RXN}^{OH})\} \approx 2$. This suggests that rate coefficient for vibrational predissociation of CH_4−OD ($2\nu_{OD}$), k_{VP}^{OD}, is much smaller than the rate coefficient for reaction and indicates a significant increase in the branching fraction for reaction. Thus, the total decay rate for CH_4−OD ($2\nu_{OD}$) will have an even larger contribution from reaction than that for CH_4−OH ($2\nu_{OH}$). It also implies that the rate coefficient for vibrational predissociation of CH_4−OD ($2\nu_{OD}$), k_{VP}^{OD}, is much smaller than that for CH_4−OH ($2\nu_{OH}$), k_{VP}^{OH}, in accord with energy gap arguments. The change in vibrational predissociation rate is likely to be greater than the observed (2-fold) change in the total decay rate upon deuteration, as seen in other OH/D systems.[20,29] The only way to determine the branching ratio definitively is to measure the inelastic and reactive scattering yields. Such experiments are planned for the future.

V. Conclusions

The pure OH/D overtone spectra of CH_4−OH/D are found to be remarkably similar to one another, with similar spectral shifts and rotational band structures. The CH_4−OH spectrum exhibits more extensive homogeneous line broadening than seen for CH_4−OD, indicating that CH_4−OH ($2\nu_{OH}$) decays about a factor of 2 more rapidly due to inelastic recoil and/or chemical reaction than CH_4−OD ($2\nu_{OD}$). The OH ($v = 1$) fragments from vibrational predissociation of CH_4−OH ($2\nu_{OH}$) have minimal rotational excitation, while the OD ($v = 1$) fragments from CH_4−OD ($2\nu_{OD}$) are highly rotationally excited. These changes in the OH/D product state distributions demonstrate that the dominant inelastic decay channel involves near-resonant vibrational energy transfer to the pentad of CH_4 vibrational states near 3000 cm^{-1} for CH_4−OH, and a less energetically favorable transfer to low-frequency bending modes of CH_4 for CH_4−OD. The larger energy gap associated with inelastic decay of CH_4−OD ($2\nu_{OD}$) implies a slower rate of vibrational predissociation, suggesting that more time will be available for reaction within the vibrationally activated complex.

Acknowledgment. This research has been supported by the Office of Basic Energy Sciences of the Department of Energy, with partial equipment support from the Chemistry Division of the National Science Foundation. The authors thank György Lendvay (Hungarian Academy of Science) for performing high level ab initio calculations on the structure and stability of various conformers of the reactant complexes between CH_4 and OH/D (manuscript in preparation).

References and Notes

(1) Tsiouris, M.; Wheeler, M. D.; Lester, M. I. *Chem. Phys. Lett.* **1999**, *302*, 192−198.
(2) Wheeler, M. D.; Tsiouris, M.; Lester, M. I.; Lendvay, G. *J. Chem. Phys.* **2000**, *112*, 6590−6602.
(3) Tsiouris, M.; Wheeler, M. D.; Lester, M. I. *J. Chem. Phys.* **2001**, *114*, 187−196.
(4) Previously, the intermolecular bond length was reported as 3.7 Å (ref 2), which arises from a pseudo-diatomic estimate rather than the true distance between the centers of mass of CH_4 and OH.; see ref 20 for a detailed explanation.
(5) Legon, A. C.; Roberts, B. P.; Wallwork, A. L. *Chem. Phys. Lett.* **1990**, *173*, 107−114.
(6) Ohshima, Y.; Endo, Y. *J. Chem. Phys.* **1990**, *93*, 6256−6265.
(7) Legon, A. C.; Wallwork, A. L. *J. Chem. Soc., Faraday Trans.* **1992**, *88*, 1−9.
(8) Atkins, M. J.; Legon, A. C.; Wallwork, A. L. *Chem. Phys. Lett.* **1992**, *192*, 368−374.
(9) Lee, E. P. F.; Wright, T. G. *J. Chem. Soc., Faraday Trans.* **1998**, *94*, 33−38.
(10) Chandra, A. K.; Nguyen, M. T. *J. Phys. Chem. A* **1998**, *102*, 6865−6870.
(11) Hashimoto, T.; Iwata, S. *J. Phys. Chem. A* **2002**, *106*, 2652−2658.
(12) Yamasaki, K.; Watanabe, A.; Kakuda, T.; Ichikawa, N.; Tokue, I. *J. Phys. Chem. A* **1999**, *103*, 451−459.
(13) Gierczak, T.; Talukdar, R. K.; Herndon, S.; Vaghjiani, G. L.; Ravishankara, A. R. *J. Phys. Chem. A* **1997**, *101*, 3125−3134.
(14) Silvente, E.; Richter, R. C.; Hynes, A. J. *J. Chem. Soc., Faraday Trans.* **1997**, *93*, 2821−2830.
(15) Glass, G. P.; Endo, H.; Chaturvedi, B. K. *J. Chem. Phys.* **1982**, *77*, 5450−5454.
(16) Miller, R. E.; Heijmen, T. G. A.; Wormer, P. E. S.; van der Avoird, A.; Moszynski, R. *J. Chem. Phys.* **1999**, *110*, 5651−5657.
(17) Nyman, G.; Clary, D. C. *J. Chem. Phys.* **1994**, *101*, 5756−5771.
(18) Clavelin, J.-L.; Mirabel, P. *J. Chim. Phys.* **1979**, *76*, 533−537.
(19) Bonn, R. T.; Wheeler, M. D.; Lester, M. I. *J. Chem. Phys.* **2000**, *112*, 4942−4951.
(20) Tsiouris, M.; Pollack, I. B.; Leung, H. O.; Marshall, M. D.; Lester, M. I. *J. Chem. Phys.* **2002**, *116*, 913−923.
(21) Brown, L. R.; Margolis, J. S. *J. Quant. Spectrosc. Radiat.* **1996**, *56*, 283−294.
(22) Rothman, L. S.; Rinsland, C. P.; Goldman, A.; Massie, S. T.; Edwards, D. P.; Flaud, J. M.; Perrin, A.; Camy-Peyret, C.; Dana, V.; Mandin, J. Y.; Schroeder, J.; McCann, A.; Gamache, R. R.; Wattson, R. B.; Yoshino, K.; Chance, K. V.; Jucks, K. W.; Brown, L. R.; Nemtchinov, V.; Varanasi, P. *J. Quant. Spectrosc. Radiat.* **1998**, *60*, 665−710.
(23) Clyne, M. A. A.; Coxon, J. A.; Fat, A. R. W. *J. Mol. Spectrosc.* **1973**, *46*, 146−170.
(24) Abrams, M. C.; Davis, S. P.; Rao, M. L. P.; Engleman, R., Jr. *J. Mol. Spectrosc.* **1994**, *165*, 57−74.
(25) Western, C. M. PGOPHER spectral simulation program Bristol, 1998.
(26) Coxon, J. A. *Can. J. Phys.* **1980**, *58*, 933−949.
(27) Dayton, D. C.; Block, P. A.; Miller, R. E. *J. Phys. Chem.* **1991**, *95*, 2881−2888.
(28) Bohac, E. J.; Miller, R. E. *Phys. Rev. Lett.* **1993**, *71*, 54−57.
(29) Pollack, I. B.; Tsiouris, M.; Leung, H. O.; Lester, M. I. Manuscript in preparation.
(30) Hossenlopp, J. M.; Anderson, D. T.; Todd, M. W.; Lester, M. I. *J. Chem. Phys.* **1998**, *109*, 10707−10718.
(31) Guyer, D. R.; Hüwel, L.; Leone, S. R. *J. Chem. Phys.* **1983**, *79*, 1259−1271.
(32) Altkorn, R.; Zare, R. N. *Annu. Rev. Phys. Chem.* **1984**, *35*, 265−289.
(33) Beswick, J. A.; Jortner, J. *Chem. Phys. Lett.* **1977**, *49*, 13−18.
(34) Beswick, J. A.; Jortner, J. *Adv. Chem. Phys.* **1981**, *47*, 363−506.
(35) Marshall, M. D.; Pond, B. V.; Hopman, S. M.; Lester, M. I. *J. Chem. Phys.* **2001**, *114*, 7001−7012.
(36) Dobbs, K. D.; Dixon, D. A.; Komornicki, A. *J. Chem. Phys.* **1993**, *98*, 8852−8858.
(37) Gonzalez, C.; McDouall, J. J. W.; Schlegel, H. B. *J. Phys. Chem.* **1990**, *94*, 7467−7471.